Imaging-Based Metrics Drawn from Visual Perception of Haze and Clarity of Materials. I. Method, Analysis, and Distance-Dependent Transparency

Author(s):
Busato, Stephan; Kremer, Daniel; Perevedentsev, Aleksandr

Publication date:
2021-05

Permanent link:
https://doi.org/10.3929/ethz-b-000485896

Originally published in:
Macromolecular Materials and Engineering 306(5), https://doi.org/10.1002/mame.202100045

Macromolecular Materials and Engineering
www.mme-journal.de

Imaging-Based Metrics Drawn from Visual Perception of Haze and Clarity of Materials. I. Method, Analysis, and Distance-Dependent Transparency

Stephan Busato, Daniel Kremer, and Aleksandr Perevedentsev**

A versatile imaging-based method is presented for quantifying the transparency of materials based on "illumination diffusion" (ID), representing scattering- and refraction-induced change in the spatial distribution of transmitted light intensity. Samples are backlit through a graticule mask, with analysis performed by comparative evaluation of graticule images recorded as-is and viewed through a sample, mimicking visual perception. ID-haze is quantified as the reduction of contrast, while ID-sharpness is derived from imaged knife-edge acuity. Measurements are performed for diverse materials, including clarified polyolefins, silica-filled amorphous polymers, semicrystalline films, and etched polymer sheets. Comparisons with the respective haze and clarity values obtained using a common ASTM D1003 haze-meter are made in terms of their quantitative correlation and suitability for applications. In particular, unlike conventional instruments, ID-based analysis captures the variation of transparency with sample-to-object "airgap" distance. Gratifyingly, ID-haze generally features a one-to-one correlation with standard ASTM haze, when determined at a specific distance. The presented method also enables sensitive detection of local defects—differentiating them from large-area characteristics—and accurately extracts the contribution of luminescence to loss of transparency. ID-based method therewith offers unique opportunities for application- and airgap-specific transparency analysis, and advanced options for optical process- and quality control.

1. Introduction

Optical transparency of materials is a key property for a wide range of applications such as displays, glass replacement, and optics, as well as ordinary packaging.[1–3] It characterizes the ability of light to pass through a material without substantial scattering, which otherwise obscures the features of objects located behind the material as seen by the observer. It is generally accepted that a single metric is insufficient for comprehensively quantifying transparency. Rather, at least two separate metrics are required for distinguishing scattering at high and low angles, respectively, each having a distinct impact on the perceived image quality.[3]

Quantifying the turbid ("milky") appearance of materials is particularly important for polymers and composites thereof. For this, the ASTM D1003 test method has been the standard for many years, employing an instrument consisting of a collimated light source impinging on the sample and an integrating sphere to differentiate specular and diffuse light transmission. From this a limited, but admittedly convenient single-value "haze" index is derived, which is defined as the percentage of transmitted light that is scattered at arbitrarily selected angles >2.5° from the optical axis.[4] Haze in polymers can be inherent to the specific materials (semicrystalline microstructure, blend composition) or result from processing (orientation, surface texture from flow instabilities, wear of calenders or molds, etc.) and end-use (contamination, abrasion).[1,5–10]

A low value of haze is typically desired for packaging materials, allowing the consumer to clearly see and appraise a product.[2,3,11] The opposite, i.e., high haze, is often sought for applications in optics such as light-management layers

Dr. S. Busato
Department of Materials
Eidgenössische Technische Hochschule (ETH) Zürich
Vladimir-Prelog-Weg 5, Zürich 8093, Switzerland
E-mail: stephan.busato@alumni.ethz.ch

The ORCID identification number(s) for the author(s) of this article can be found under https://doi.org/10.1002/mame.202100045.

DOI: 10.1002/mame.202100045

Dr. D. Kremer
Department of Macromolecular Chemistry I
University of Bayreuth
Universitätsstr. 30, Bayreuth 95447, Germany

Dr. A. Perevedentsev
Light Technology Institute
Karlsruhe Institute of Technology
Engesserstr. 13, Karlsruhe 76131, Germany
E-mail: perevedentsev@kit.edu

Dr. A. Perevedentsev
InnovationLab
Speyererstr. 4, Heidelberg 69115, Germany

for display and photovoltaic technologies.[12–14] Hence, accurate quantification of transparency in terms of haze is of principal importance for research and development of novel materials, as well as determining the suitability of a given material for specific applications and quality control.

Despite its prevalent use to-date, the limitations and shortcomings of ASTM D1003 have become apparent in recent years. In particular, the correlation of haze with visual perception has been questioned since, for example, materials with nominally equal haze values can exhibit substantially different angular distributions of scattered light, which naturally correspond to observable differences in transparency.[15–18] Due to the specific instrument geometry prescribed by the current standard, haze is independent of sample placement along the optical axis—that is, clearly contrary to the common visual observation of improved material transparency when placed in contact with an object. Adding to the confusion, selected ASTM D1003 haze-meters additionally measure "clarity" using a non-standardized[19–21] definition for light scattered at low angles (generally correlating with the ability to resolve fine object details), according to which the clarity of a material does vary with sample placement. This presents one with difficulties in reconciling haze and clarity into a meaningful measure of transparency that correlates with visual perception. Finally, the typical haze-meter provides only a single spatially-averaged value for a ≈5 cm^2 area, which renders it particularly unsuitable for analysis of heterogeneous/patterned samples[22,23] or accurate identification of local defects in quality control applications.[10] Reflective of these limitations of the ASTM D1003 is the fact that recent reports on analysis of thin-film materials have increasingly resorted to alternative, non-standardized measurements for haze.[24–30]

Recognizing the above-mentioned lack of a comprehensive analysis, an alternative imaging-based method[31] was recently put forward. In this approach, a backlit mask was photographically imaged as-is and with a sample placed in direct contact. The mask generated a precisely defined spatial pattern of illumination light intensities, the characteristics of which were altered upon passing through a turbid material and subsequently analyzed via the corresponding modulation transfer functions (MTFs). "Imaging haze", therefore, was quantified using a practically relevant definition based on the reduction of perceived image quality for an object (here: a mask) viewed through a turbid material.[31]

In the present work, we report an advanced extension of this method for providing a complete quantitative description of in-contact and distance-dependent transparency of materials, and describe the practice and advantages thereof. An updated, versatile definition of transparency is provided in terms of "illumination diffusion" (ID) induced by a material sample, and is quantified in terms of ID-haze and ID-sharpness. Measurements are performed using a commercial instrument developed by Rhopoint Instruments Ltd. on a wide range of materials—including clarified polyolefins, filled amorphous polymers, and etched polymer sheets—and the results compared throughout with those obtained using a conventional haze-meter.

2. Experimental Section

2.1. Materials

Propylene-ethylene random copolymer ("PP"; RD208CF, C2 content ≈ 7 mol%) was purchased from Borealis. Polystyrenes (PS 165H and PS 143H) were purchased from BASF. Linear-low-density polyethylene (PE) ("LLDPE"; DOWLEX 2552E) was purchased from The Dow Chemical Company, USA. The clarifying agent 1,2,3-trideoxy-4,6:5,7-bis-O-[(4-propylphenyl) methylene]-nonitol ("NX8000") was purchased from Milliken Chemical Co., USA. Graphite (grade 4124; mean particle size <3 µm) was purchased from Asbury Carbon, USA. Poly(methyl methacrylate) ("PMMA") sheets (0.25 mm thickness) were purchased from Röhm GmbH, Germany.

2.2. Sample Fabrication

Circular plaque samples (1.1 mm thickness, 26.6 mm diameter) of various polymer:additive blends were prepared as described in previous reports.[31–33] Polymer and additive powders were dry-mixed at the required concentrations, and fed into a laboratory co-rotating mini-twin-screw extruder (XploreVR MC 15, Xplore Instruments BV, The Netherlands) operated at 260 °C (PS-based blends) and 240 °C (LLDPE- and PP-based blends), unless noted otherwise. After compounding for ≈5 min at 40 rpm under nitrogen blanket, the molten blends were extruded into a laboratory micro injection molder (XploreVR IM 12, Xplore Instruments BV, The Netherlands) kept at the respective temperature, and finally injected into a plaque mold held at 20 °C. In each case, polymer:additive concentration series were produced by successively diluting the compounded blend by adding the required amount of neat polymer after each extrusion step. These optimized processing conditions yielded plaques that exhibited negligible curvature or warp. PMMA sheets with a varying degree of surface roughness (root mean square (RMS) roughness ranging from 4 to 190 nm) were fabricated using a wet etching process, the details of which will be reported elsewhere.

2.3. Characterization

Imaging-based analysis of transparency was performed with a Rhopoint ID-TX imaging transmission appearance meter (Rhopoint Instruments Ltd., UK; **Figure 1**).[34] As its principal components, the instrument comprises an LED light source (color temperature = 5500 K), a polytetrafluoroethylene sheet acting as diffuser, a lens for collecting transmitted light (f = 25 mm; focused on the graticule) and a camera (monochrome sensor; 1280 × 1024 pixels), providing ≈81 px mm^{-1} imaging resolution on the graticule. The graticule comprises a 3 × 2 checkerboard array of fully opaque squares (4 × 4 mm^2; sputtered chromium overcoated with a low-reflectivity chromium oxide layer) on a glass substrate. The graticule thus provides seven regions of interest ("ROIs"; four horizontal and three vertical; dimensions = 6.57 × 1.85 mm^2) that capture the transitions between adjacent opaque and transparent graticule areas. The

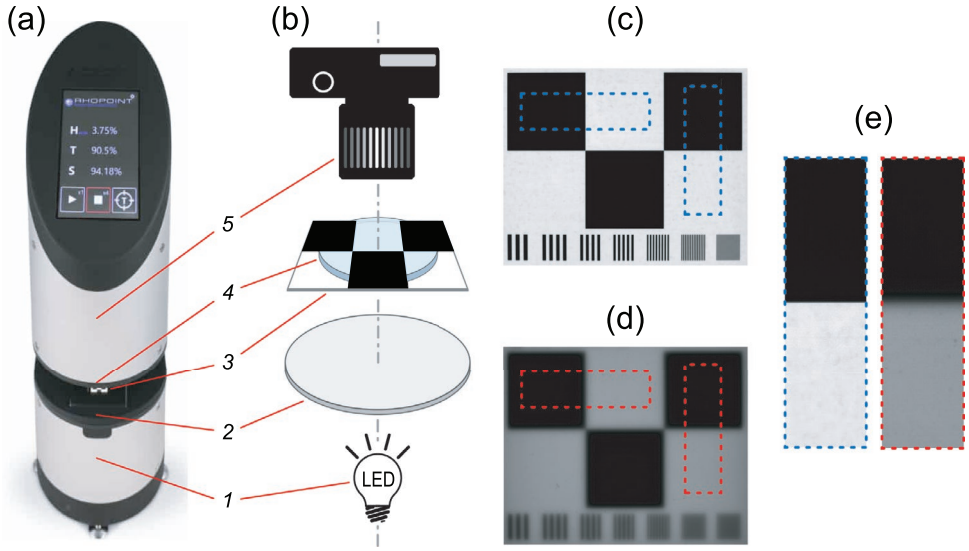

Figure 1. a) Photograph of the Rhopoint ID-TX instrument (height = 47 cm) and b) schematic illustration of its principal components arranged on the optical axis: 1) light source, 2) diffuser, 3) graticule, 4) sample, and 5) camera. Also shown are the images of the graticule (dimensions of each square = 4 × 4 mm^2) taken c) without sample ("reference") and d) with a turbid sample placed in contact, where the dotted lines indicate selected ROIs for which optical data is extracted. e) Expanded views of the respective ROIs. Image in (a) reproduced with permission;[34] Copyright 2019, Rhopoint Instruments Ltd.

instrument was factory-calibrated against a 30% ASTM haze standard (pre-calibration $H_{ID}(8)$ reading ≈ 27.5%). Measurements were performed by placing the samples atop the graticule—in contact, or at a predetermined airgap distance set by spacers—followed by image acquisition and data processing using the instrument's built-in software (total measurement time <1 s). (*N.B.* Alternative software packages for extracting ESF and MTF data for a knife-edge were freely available.[35–36]) Unless specified otherwise, all reported values were the averages of data measured for seven ROIs. Further details of hardware and analysis will be provided in the following sections.

Haze in accordance with ASTM D1003 (hereafter: "ASTM haze") was measured using a conventional haze-meter instrument (Haze-Gard Plus, equipped with CIE Standard Illuminant C; BYK Gardner GmbH, Germany). The same instrument also allowed for the measurement of "clarity", that is, the low-angle scattering of transmitted light that can be evaluated at angles of less than 2.5°.[37] Topography analysis was performed with a KLA Tencor D-500 stylus profilometer. A 2 mm scan length was used, with 3–4 scans performed on different areas for a given sample (average RMS roughness values were accurate within ≈4% based on repeated measurements). UV–Vis absorption spectra were recorded using a custom-built setup comprising an AvaLight-DHS-Bal light source and an AvaSpec-ULS3648 spectrometer. Photoluminescence (PL) spectroscopy for 1.1-mm-thick plaques of LLDPE/NX8000 was performed using a Jobin Yvon Horiba Fluoromax-3 spectrofluorometer. PL spectra were recorded with the excitation wavelength (375 nm) matching the absorption maximum of the whitener in commercial NX8000. PL excitation (PLE) spectra were recorded for emission wavelength (431 nm) that coincides with the PL maximum, with the resulting PLE spectra thereby effectively recreating the corresponding absorption spectra.[38]

3. Results and Discussion

3.1. Instrumentation

The instrument for imaging-based analysis of transparency is represented in Figure 1a,b.[34] Conceptually, it is designed to replicate the practically encountered conditions for ocular evaluation of transparency. Hence, it comprises an LED white light source, the output of which is passed via a diffuser to generate diffuse, rather than collimated, illumination that approximates the typical ambient lighting. The illumination light is then directed onto a graticule (Figure 1c), comprising alternatingly opaque and transparent 4 × 4 mm^2 squares, that is, an array of knife-edge optical elements. The function of the graticule is to generate a well-defined spatial pattern of light intensity, with sharp transitions between backlit and masked areas—essentially representing an object viewed by the observer. Finally, a camera focused on the graticule is used to record an image of the transmitted light.

Placing a turbid sample between the graticule and the camera/observer leads to illumination diffusion (ID)—that is, redistribution of the spatial pattern of light intensity generated by the graticule due to "diffusive" light scattering by the sample. To illustrate this, Figure 1c and Figure 1d compare images of the graticule recorded without a sample (hereafter referred to as the "reference") and with a turbid polymer film placed in direct contact with the graticule, respectively (expanded views are also shown in Figure 1e). Evidently, the presence of the sample leads to a reduction of contrast between backlit and masked areas, as well as a blurring of the transitions between them. Quantitative analysis of transparency thus relies on comparing the image of the graticule viewed through a given sample with the reference image of the bare graticule using, in both cases, data from

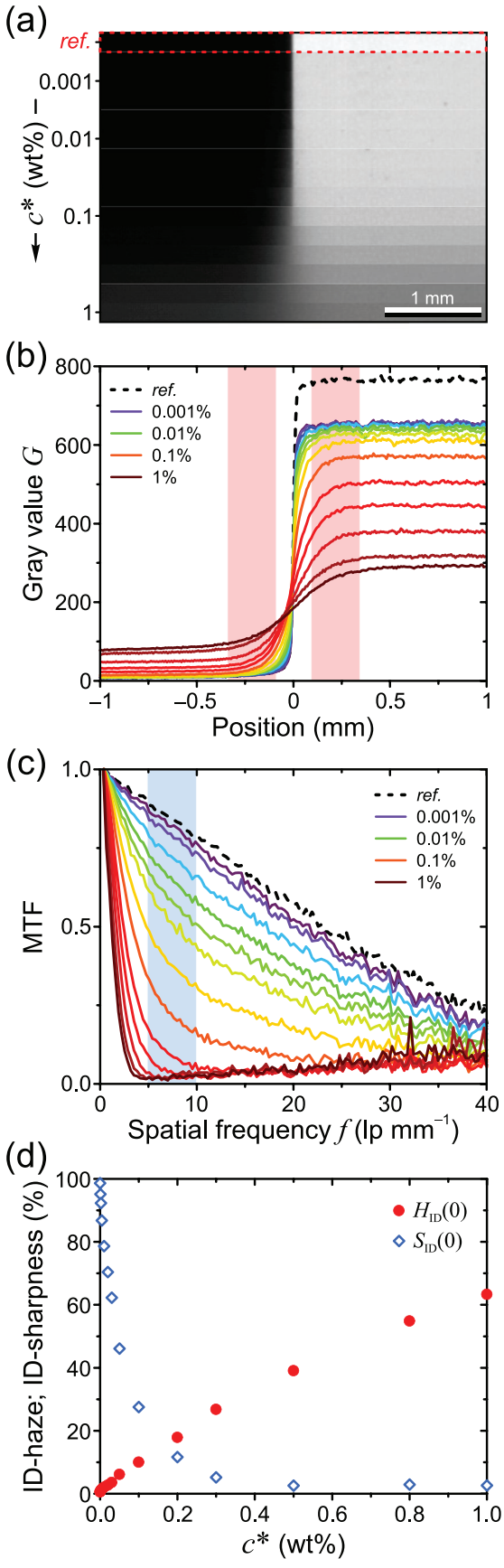

selected ROIs centered on backlit-to-masked transitions, two of which are shown in Figure 1c–e.

3.2. Analysis

Analysis of transparency using ID will be described below using exemplary imaging data recorded for PS plaques filled with varying fractions of a silica scatterer to cover a maximally wide range of ASTM D1003 haze (2–100%) and clarity (99–0%) values. ID-based analysis was performed for samples placed in contact with graticule. Representative selected-area images for a single horizontally-oriented ROI are shown in **Figure 2**a as a function of scatterer concentration, c^*, to provide a visual counterpart to the optical data.

ASTM D1003 defines "haze" for a given material specimen in qualitative terms as "the reduction in contrast of objects viewed through it".[4] Here, however, instead of resorting to a numerical evaluation based on an arbitrary minimum light scattering angle, we use a definition of contrast that is widely employed in imaging applications[39,40] and human vision studies[41,42]—namely the so-called Michelson contrast, expressed as $(L_{max} - L_{min})/(L_{max} + L_{min})$ where L is maximum or minimum luminance.

The edge spread function (ESF), representing the spatial distribution of light intensity and expressed as a profile of average gray value G as a function of position, is then extracted for each ROI. The resulting ESFs are presented in Figure 2b. Increasing c^* clearly leads to a progressive attenuation of the relative difference in light intensity for the backlit (bright) and masked (dark) areas in the vicinity of the "edge" (the transition between backlit and masked areas). To calculate contrast, the data within ±90 µm of the center of the edge is excluded, and the gray values G of backlit and masked ESF regions are averaged within 250 µm regions adjacent to the excluded region, as illustrated in Figure 2b. Note that exclusion of the edge is necessary to maximally decouple the optical effects of haze (variation of contrast) and sharpness (variation of edge slope), as will be shown below. The specific ranges used for excluding and averaging ESF data were selected following judicious optimization, and recalling that ocular evaluation of contrast relies on saccadic sampling in close proximity to a local change in luminance.[43]

Contrast C for a given ROI is calculated as:

$$C = \frac{\langle G \rangle_{\text{backlit}} - \langle G \rangle_{\text{masked}}}{\langle G \rangle_{\text{backlit}} + \langle G \rangle_{\text{masked}}} \quad (1)$$

Figure 2. Exemplary analysis of ID-haze (H_{ID}) and ID-sharpness (S_{ID}) for PS plaques containing varying concentrations, c^*, of a silica scatterer, spanning ASTM D1003 haze range = 2–100% and "clarity" range = 99–0%. a) Stacked selected-area ROI images, showing the evolution of transparency as a function of c^*. The reference image for the graticule is highlighted. Also shown are the corresponding b) ESF and c) MTF data, wherein the shaded areas indicate the data regions used for analysis and the legends denote selected c^* values. d) H_{ID} and S_{ID} values as a function of c^*. All measurements are performed for samples placed in contact with the graticule.

where $\langle G \rangle$ are the average gray values for backlit and masked regions. ID-haze, H_{ID}, is then calculated from the ratio of contrast values for the sample and "reference" (graticule-only) images as:

$$H_{ID} = \left(1 - \frac{C_{sample}}{C_{ref}}\right) \times 100\% \quad (2)$$

The resulting H_{ID} data for the PS/silica samples are shown in Figure 2d, revealing the expected sublinear increase of H_{ID} with scatterer concentration, reaching a value of 63% for $c^* = 1\%$. Gratifyingly, this trend is consistent with the corresponding images in Figure 2a, which show that some contrast between backlit and masked regions remains even at the maximum employed c^*.

Turning now to "clarity", this metric is generally understood in the field to correspond to "see-through quality", that is, resolution of fine object detail when viewed through a material specimen.[37,44] Typically, haze-meters use a ring sensor to quantify clarity as the fraction of transmitted light scattered by an angle <2.5°[19,21] instead of its standardized definition.[20] To avoid confusion, we quantify resolution of fine detail via a metric termed "*ID-sharpness*" using analysis of the corresponding modulation transfer function (MTF), as commonly employed for characterizing the quality of imaging systems and components.[45]

The MTF describes the magnitude response of an optical system to sinusoids of different spatial frequencies.[45] MTF for an optical edge (transition between areas of differing luminance) can be calculated by taking the first derivative of the corresponding ESF and applying the Fourier transform.[31,36] Hence, while the edge region in the ESF data was excluded in the previously described analysis of ID-haze, the quantitative evaluation of ID-sharpness specifically uses the edge to calculate the corresponding MTF.

The exemplary ESF data are shown in Figure 2b reveals that the nominally sharp backlit-to-masked transition becomes progressively shallow with increasing scatterer concentration, corresponding to blur and loss of object detail. This is reflected in the corresponding MTFs shown in Figure 2c in the form of the reduction of amplitude at high spatial frequencies with increasing scatterer concentration. ID-sharpness, S_{ID}, is then calculated as:

$$S_{ID} = \frac{\langle \mathrm{MTF} \rangle_{sample}}{\langle \mathrm{MTF} \rangle_{ref}} \times 100\% \quad (3)$$

where $\langle \mathrm{MTF} \rangle$ are the average MTF values in the 5–10 line pairs per millimeter (lp mm^{-1}) spatial frequency range obtained for the sample and reference images. The specific spatial frequency range is selected to coincide with the ≈6 lp mm^{-1} resolution of the human eye at a 20 cm viewing distance[46] and, therewith, correlate with visual perception of transparency.

The resulting data for the PS/silica samples (Figure 2d) shows a rapid reduction of S_{ID} with scatterer concentration. The data appears to be consistent with the corresponding images in Figure 2a, which similarly show that the increase of edge blurriness saturates for $c^* \approx 0.3\%$.

Hence, ID-based analysis of transparency utilizes the graticule-only images as a reference for 0% H_{ID} and 100% S_{ID}, as evident from Equations (2) and (3) respectively. As well as enabling visual-perception-correlated evaluation of transparency that does not rely on arbitrary light-scattering angles, this approach minimizes the effects of, for instance, graticule contamination, on the measured values. For completeness, exemplary analysis of transmittance with the present method, and its close correlation with transmittance measured using a conventional haze-meter, are presented in Figure S1, Supporting Information.

3.3. ID-Haze versus ASTM Haze

Before describing in detail the advantages of transparency analysis using the present method, the correlation between ID-based metrics with conventional ASTM haze and clarity values needs to be examined. From everyday experience with, for instance, packaging containers and laminate films, one is aware that transparency of a material specimen reduces at increasing "airgap" distance with the viewed object. Visually, haze increases with airgap distance, while sharpness simultaneously decreases. In the present method, this can be reproduced by conducting measurements for samples placed at a predetermined distance from the graticule using spacers. Hence, hereafter ID-based metrics will be specified by the airgap distance in mm units correct to one significant figure (e.g., H_{ID} at 7.9 mm airgap distance will be referred to as '$H_{ID}(8)$').

Empirically it was found that ASTM haze shows an essentially one-to-one correlation with $H_{ID}(8)$, particularly for haze values ≤30% for which the ASTM D1003 standard is applicable.[4] This is illustrated in **Figure 3** for an extraordinarily diverse selection of polymer samples, including thin semicrystalline polymer films (varying materials), PMMA films with varying surface roughness, plaques of silica-filled amorphous polymers (varying materials, plaque thickness, and scatterer size and loading), and plaques of clarified polyolefins (varying materials and loading of clarifying agent). The correlation, indeed, also holds for light-absorbing samples—namely, graphite-filled PS plaques—for which transmittance varies in the 1–89% range, depending on graphite loading. Further details of samples are provided in the Experimental Section.

Such close quantitative match between ASTM haze and $H_{ID}(8)$ may be surprising given the fundamentally different analysis principles relying, respectively, on angle-selective light-scattering and image contrast reduction. Nevertheless, it emerges that ASTM haze specifically corresponds to out-of-contact ID-haze measured at approximately 8 mm airgap. Distance-dependence of ID-haze will be examined in more detail in Section 3.5.

Finally, it is interesting to note that the largest deviation from one-to-one correlation in Figure 3 is observed for clarified polyolefins, for which $H_{ID}(8)$ is underestimated relative to ASTM haze by, on average, 10% (LLDPE/NX8000) and 3% (PP/NX8000). The possible contribution of additive luminescence to this discrepancy is investigated in Section 3.7.

3.4. ID-Sharpness versus "Clarity"

"Clarity" is a non-standardized metric for low-angle scattering of transmitted light that can be additionally measured using conventional haze-meter instruments. However, its correlation with visual perception has been questioned[37] and to-date

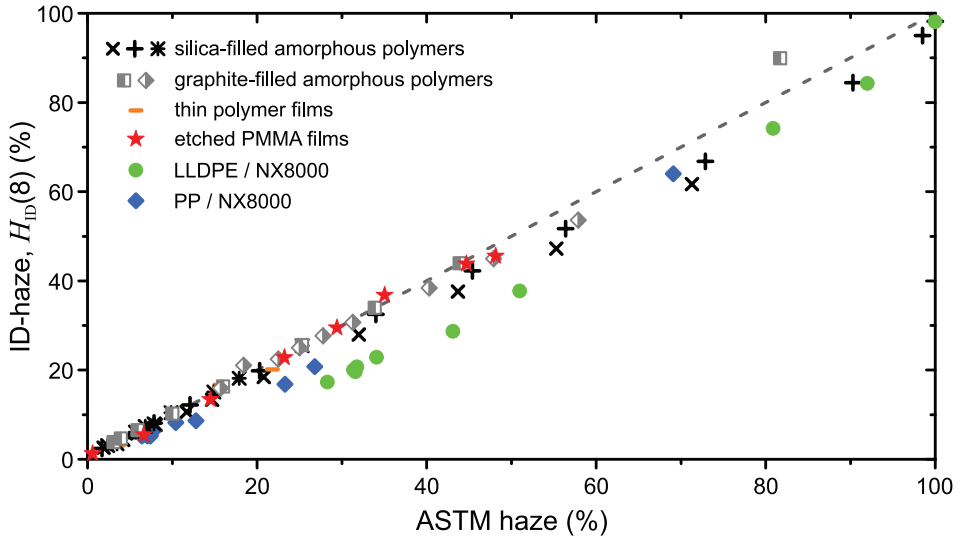

Figure 3. Comparison of ID-haze measured at 7.9 mm airgap distance, $H_{ID}(8)$, and ASTM D1003 haze for a diverse range of polymer-based samples. These include: plaques of amorphous polymers filled with silica scatterers (different scatterer size and plaque thickness; black symbols); plaques of graphite- and silica-filled amorphous polymers (transmittance spanning 1–89% range; gray semi-open symbols); commercial semicrystalline polymer films (thickness ≤ 100 µm; orange bars); etched PMMA films (RMS roughness spanning 4–188 nm; red stars), and plaques of clarified LLDPE and PP (different fractions of the NX8000 clarifying agent; green and blue symbols respectively). Dashed line is a guide to the eye for equivalent $H_{ID}(8)$ and ASTM D1003 haze.

it remains little employed in the field. Hence, clarity and its ID-based counterpart ID-sharpness are compared via their correlation with the respective ASTM haze and ID-haze metrics, as measured for the above-described range of polymer samples (Figure 3). As shown in **Figure 4**a, clarity measured using a conventional haze-meter shows minimal variation over the entire ASTM haze range, with clarity values remaining above 90% for the majority of samples, including those exhibiting high haze values up to 80%. In fact, clarity values <50% were generally only obtained for samples for which the haze-meter measured a non-physical haze value of 101% (!) (see right panel of Figure 4a). While there is no reported visual perception study to confirm that the see-through quality of such samples is only weakly affected over the entire ASTM haze range, undeniably the limited dynamic range of the clarity scale, that is, ≈10% as shown in Figure 4a, is poorly suited for applications that require and rely on sensitive optical quality control.

ID-based sharpness and haze data is shown in Figure 4b, measured in both cases at a 7.9 mm airgap distance for which, as shown previously, H_{ID} exhibits the closest match with ASTM haze. $S_{ID}(8)$ is found to decrease, essentially, continuously with increasing $H_{ID}(8)$ across the entire span of the 0–100% scale. Nevertheless, despite the differences in their absolute values, a close examination of the data for selected outliers in Figure 4a,b shows that $S_{ID}(8)$ and clarity are generally correlated (note, e.g., the data for thin films and etched PMMA samples in the 16–45% haze range). For illustration of the above, the reader is directed to Figure S3, Supporting Information, which shows a plot of $S_{ID}(8)$ as a function of clarity.

3.5. Distance-Dependent Transparency

We now turn our attention to the dependence of transparency on the airgap distance between a material specimen and a viewed object. For this particular study, PMMA films were employed, for which a controlled degree of surface roughness was generated on one of the sides by a wet etching process (see exemplary topography profiles in **Figure 5**a), thereby confining the features responsible for light-scattering to a thin, sub-micrometer surface layer.

For reference, Figure 5b shows ASTM haze and clarity as a function of RMS roughness, R_q, measured using the conventional haze-meter. (*N.B.* Identical values were obtained for light incident on pristine or etched film surfaces.) Interestingly, haze is found to increase linearly with R_q up to $R_q \approx$ 150 nm followed by an unexpected sharp roll-off. This reduction of haze at higher roughness values may appear paradoxical at first, but the data in Figure 5b also reveals a simultaneous reduction of clarity occurring in same R_q range. Taken together, these observations can be attributed to a change in the angular distribution of scattered light, with wide-angle scattering (responsible for haze) dominating for R_q < 150 nm and low-angle scattering (responsible for loss of clarity) becoming prevalent at higher roughness values. Such a change may be a combination of two factors, namely i) predominantly forward-scattering of larger particles and ii) an increasing contribution from refraction, rather than scattering, for high-roughness films.[19]

Figure 5c shows exemplary images of etched PMMA films photographed against a backdrop, wherein films are placed in contact or separated by 8 and 20 mm, revealing the strong impact of airgap distance on visually-perceived transparency. For example, despite the differences in ASTM haze and clarity values, an equivalent maximum transparency is observed for all films (R_q spanning 15–188 nm) imaged in contact with the backdrop. Transparency reduces significantly for films with R_q = 87 and 188 nm by the airgap distance of 8 mm, with the samples exhibiting a comparable degree of haze which appears to be consistent with the measured values of 29% and 35%

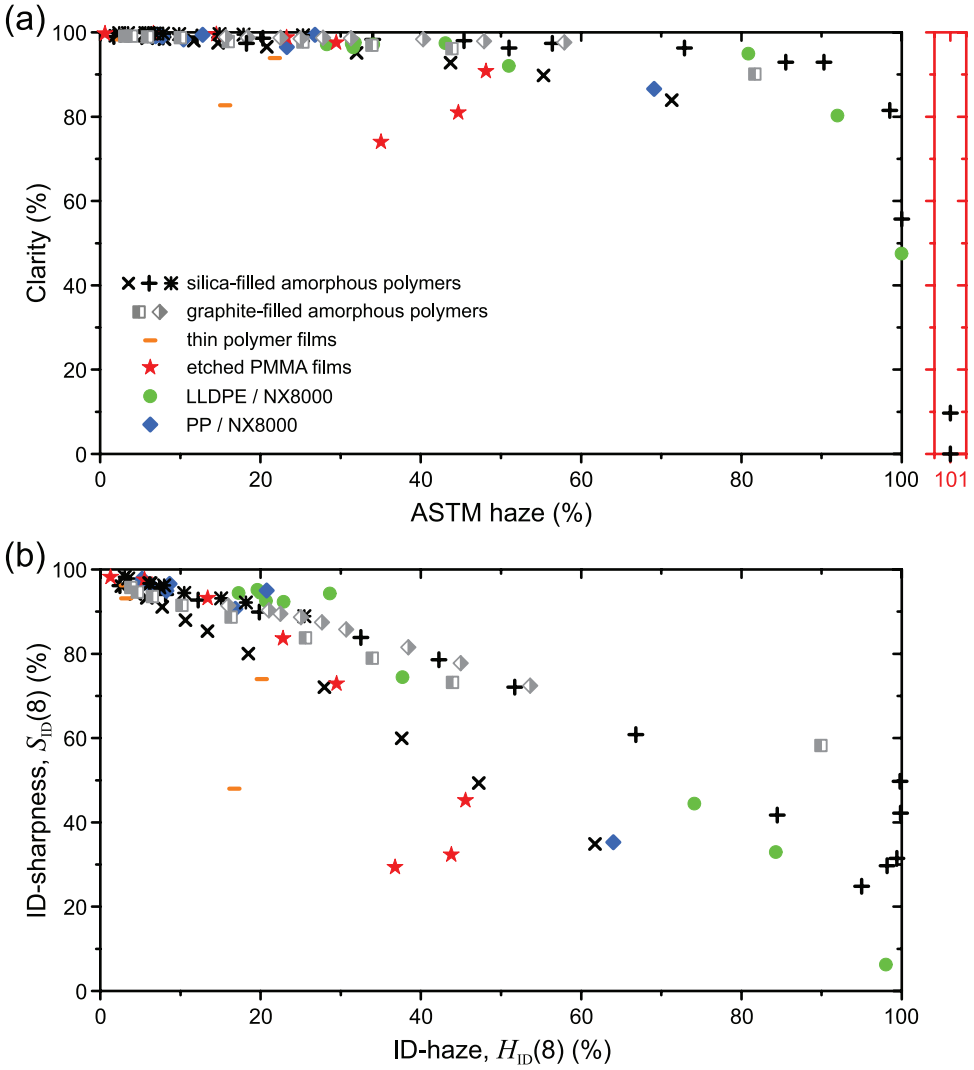

Figure 4. Correlation of a) clarity with ASTM D1003 haze and b) ID-sharpness and -haze measured at 7.9 mm airgap distance for a range of polymer-based samples (as in Figure 3). These include: plaques of amorphous polymers filled with silica scatterers (different scatterer size and plaque thickness; black symbols); plaques of graphite- and silica-filled amorphous polymers (transmittance spanning 1–89% range; gray semi-open symbols); commercial semicrystalline polymer films (thickness ≤ 100 µm; orange bars); etched PMMA films (RMS roughness spanning 4–188 nm; red stars), and plaques of clarified LLDPE and PP (different fractions of the NX8000 clarifying agent; green and blue symbols respectively). The right panel in (a) shows an expanded view centered on haze = 101%, as measured by the haze-meter.

respectively. However, with a further increase of airgap distance to 20 mm the film with R_q = 188 nm is appreciably more hazy than the film with R_q = 87 nm, with the respective images in Figure 5c exhibiting "smudged" colors of lesser contrast for the former sample. Hence, it is unambiguously demonstrated that the conventional single-value haze and clarity metrics provide an incomplete, if not erroneous, characterization of transparency by entirely omitting its variation with the airgap distance.

While by constraint of the measurement geometry, a conventional haze-meter cannot quantify the distance-dependence of haze and clarity, ID-based analysis comprehensively reproduces the variation of transparency with airgap. This is illustrated in **Figure 6** by exemplary ID-haze data for the same series of etched PMMA films.

Figure 6a shows H_{ID} as a function of airgap distance for films of different roughness. Consistent with the images shown in Figure 5c, an equivalent H_{ID} < 1% is obtained for all films when analyzed in contact with the graticule, with H_{ID} then increasing with airgap distance to an extent that is proportional to film roughness. Interestingly, while for the films with R_q < 90 nm ID-haze appears to roll off to a plateau value with increasing airgap — i.e., H_{ID} at 9.6 mm is within ≈2% absolute of the respective values at 20 mm — this is much less pronounced for the film with R_q = 188 nm ($H_{ID}(10)$ = 42%; $H_{ID}(20)$ = 60%). By inspection of data for a large number of samples, it was found that the extent to which H_{ID} plateaus with the airgap distance depends on the corresponding ID-sharpness (or clarity) values—that is, maximal sharpness/clarity values lead to a more prominent saturation of H_{ID} with distance. This

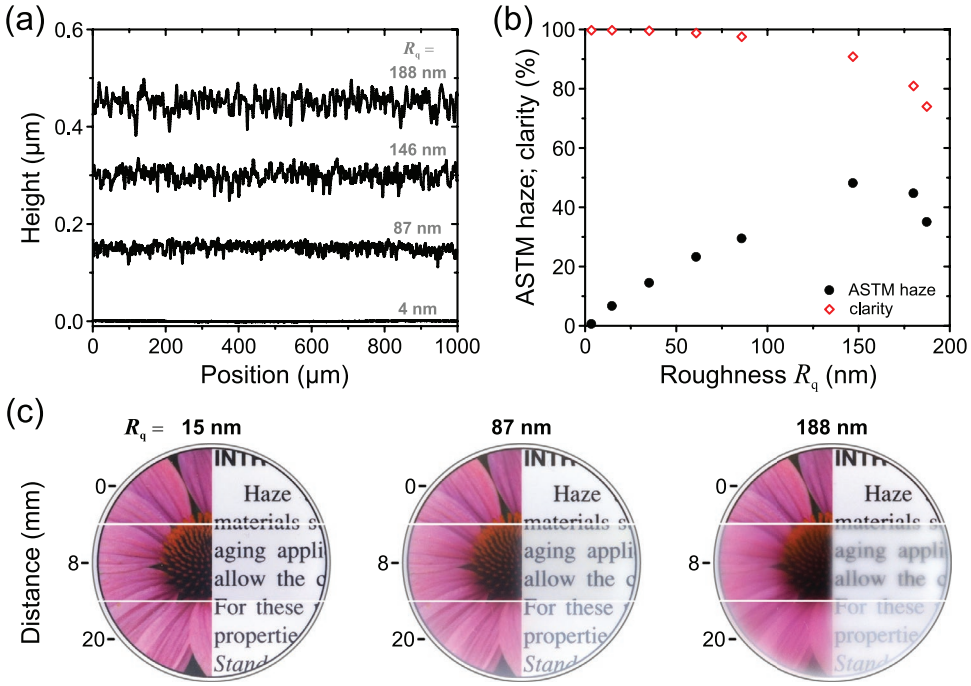

Figure 5. Optical properties of etched PMMA films. a) Representative topography profiles with RMS roughness values, R_q, indicated. Data are offset along the ordinate axis. b) ASTM haze and clarity as a function of R_q. c) Stacked images of a backdrop viewed through films of different roughness (R_q as indicated) placed at different airgap distances (0, 8, and 20 mm), with the etched side facing the backdrop.

can be clearly seen, for instance, in Figure 6a for films with R_q = 87 and 188 nm (clarity = 97% and 73% respectively), with the latter exhibiting a continuous increase of H_{ID} up to the highest airgap distance. Gratifyingly, this is corroborated by the corresponding images shown in Figure 5c, which highlight that haze at 8 and 20 mm airgaps is approximately constant for the film with R_q = 87 nm, while increasing significantly for the film with R_q = 188 nm within the same airgap range.

Figure 6b shows ID-haze as a function of roughness measured at selected airgap distances. As noted previously, H_{ID} at 7.9 mm airgap shows excellent correlation with ASTM haze for all samples, thus indicating that the ASTM D1003 metric used to-date specifically corresponds to haze at large airgap distances. However, much smaller airgaps are often encountered in packaging applications. The data in Figure 6b also shows that for samples with R_q in the 15–146 nm range $H_{ID}(0.7)$ remains constant at 3.3 ± 0.5% despite the corresponding ASTM haze values varying from 7 to 48%. Hence, although the accompanying optical model is yet to be developed,[9] ID-based analysis of the distance-dependence of haze can enable accurate material selection and transparency specification for practically relevant airgaps.

To further illustrate the above beyond the example of etched PMMA films, **Figure 7** shows ID-haze and ID-sharpness for two commercial semicrystalline polymer films, that is, polyethylene (PE) and polyethylene terephthalate (PET), as a function of airgap distance. The respective H_{ID} and S_{ID} profiles are found to cross-over at intermediate airgaps, implying that selecting the material with highest transparency depends on the end-product-intended airgap, as well as the relative importance of reproducing vivid colors or resolution of detail. Thus, for instance, the 50-μm-thick PET film exhibiting lower H_{ID} in the 12–20 mm airgap range and higher S_{ID} in the 1–20 mm airgap range is best suited for applications utilizing intermediate-to-large airgap distances. On the contrary, the 78-μm-thick PE film offers superior transparency for close-contact applications, featuring improved H_{ID} and S_{ID} for 0–12 and 0–1 mm airgaps, respectively. Clearly, the corresponding single-point haze-meter data for the same films, indicated by the arrows in Figure 7, offers no equivalent opportunity for optimal material selection and end-product design. Finally, we note that the presented ID-haze and ID-sharpness data exhibit a continuous variation with airgap distance, confirming accurate placement of these thin and flexible polymer films in terms of airgap.

3.6. Local Defects

Analysis of haze is often performed on-line as a means for optical quality control of polymer articles.[10] The typical defects encountered in the field arise due to production process faults, resulting in, for example, "fish eyes", air bubbles in laminates, crystallization and orange peel, as well as contaminants. Elsewhere, tooling wear can also lead to defects and inhomogeneities such as die lines and surface roughness. Such defects would be manifested as a modified—typically increased—local haze reading.

In order to compare the capability of the ID-based instrument and a conventional haze-meter for identifying such local defects, analysis was performed on locally etched PMMA films that feature high-roughness spots

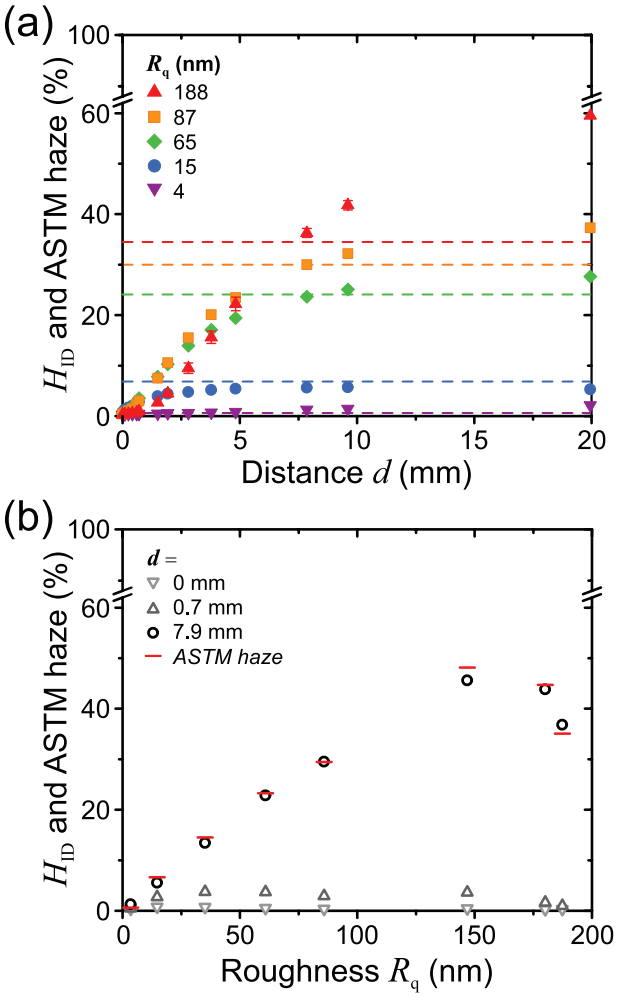

Figure 6. H_{ID} and ASTM D1003 haze of etched PMMA films. a) Data for selected films (roughness R_q as indicated) as a function of airgap distance d. Dashed horizontal lines indicate the corresponding ASTM haze values. b) Data measured at selected distances (0, 0.7, and 7.9 mm; open symbols) as a function of R_q, and the corresponding ASTM haze values (—).

(R_q = 43–192 nm, compared with ≈4 nm for the pristine films) approximately 3–7 mm in diameter. Such surface roughness defects can be readily encountered in, for instance, blown PE films due to melt flow disturbance at the die or stress-induced crystallization.[5] Images of the films taken against a Siemens star backdrop at 8 mm airgap are shown in **Figure 8**a. These images reveal a conspicuous local loss of contrast for the defect areas (highlighted) that is proportional to the roughness thereof.

ID-based analysis employs a graticule which, in the present example, provides seven ROIs containing backlit-to-masked transitions that are used for quantifying transparency (Figure 1c). Hence, a single image yields ID-haze, sharpness, and transmittance data evaluated at seven individual ROIs within a 12 × 8 mm^2 area. Figure 8b shows ID-haze and sharpness values for the locally etched PMMA films measured at the 7.9 mm airgap distance (i.e., the distance at which H_{ID} shows optimal quantitative match with ASTM haze), reporting the individual values

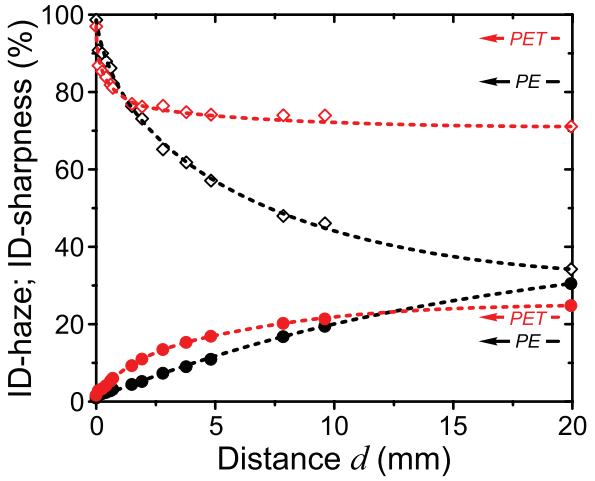

Figure 7. ID-haze (solid symbols) and ID-sharpness (open symbols) as a function of distance for commercial PE (thickness = 78 µm; black symbols) and PET (thickness = 50 µm; red symbols) films. Dotted lines provide a guide to the eye. The arrows indicate the corresponding ASTM D1003 haze and clarity values (lower and upper arrow pairs, respectively).

obtained for all seven ROIs. As expected, the reference pristine films feature ID-haze and ID-sharpness values that are closely distributed around the mean: $H_{ID}(8)$ = 1.3 ± 0.5% and $S_{ID}(8)$ = 98.4 ± 0.6%. On the contrary, the locally etched PMMA films in all cases feature a single outlier datapoint exhibiting higher ID-haze and lower ID-sharpness, wherein the difference correlates with the specific defect roughness and diameter.

A conventional haze-meter quantifies haze and clarity as a single value averaged over a ≈25-mm-diameter area, defined by the size of the illumination spot and the aperture of the integrating sphere. That is, a single ASTM haze or clarity value is obtained for an area that is more than 35-fold larger than the dimensions of a single ROI in the ID-based measurement. Illustrating the implications of the above, ASTM haze and clarity data measured for the same series of locally etched PMMA films are shown in Figure 8c. ASTM haze shows only a minor variation with local roughness. For instance, a low value of 1.2% is measured for the film with a local maximum R_q value of 43 nm (compare with maximum $H_{ID}(8)$ of, *nota bene*, 13% in Figure 8b) that is virtually indistinguishable from the corresponding value for the pristine film (0.6%). This is fully expected given that a 3-mm-diameter defect constitutes only ≈1% of the total measured sample area. Moreover, the conventional haze-meter data does not differentiate between local and homogeneously-distributed haze. Finally, due to the above-noted limited dynamic range of the clarity scale (Figure 4a), the clarity values obtained with that instrument remain above 99% for all samples.

Thus, the single-value haze and clarity measured with a conventional haze-meter are found to provide limited opportunities for sensitive optical quality control and detection of local defects compared with ID-based analysis. In the case of the latter, the effective sensitivity can be even further enhanced by performing measurements at higher airgap distances, for example, 20 mm, as illustrated in Figure 6a.

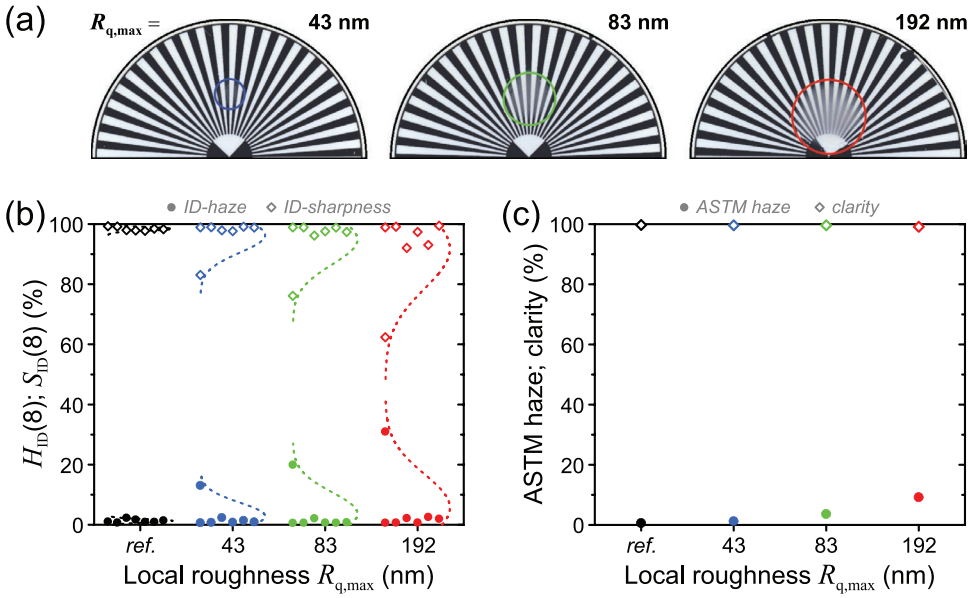

Figure 8. a) Images of a Siemens star backdrop viewed through PMMA films (nominal $R_q \approx 4$ nm; placed at 7.9 mm airgap distance) pre-patterned with circular "defect" areas of high local roughness, $R_{q,max}$ (as indicated; defect diameters ≈3–7 mm). b) ID-haze and ID-sharpness data (solid circles and open diamonds, respectively) for the samples measured at 7.9 mm airgap distance showing, in each case, the values for all seven ROIs obtained from a single image. Dotted lines represent the corresponding normal distributions for each dataset, overlaid as a guide to the eye. c) ASTM haze and clarity data (solid circles and open diamonds, respectively) for the same samples. In both cases, data is also shown for the pristine, "reference" PMMA film (black symbols and lines).

3.7. Impact of Specimen Luminescence

To-date specimen luminescence has rarely been considered as a possible contributing factor to loss of transparency, although some reports have indicated that it can indeed lead to, for instance, deviation of the measured haze values.[29,47] However, many of the commercial polymer additives often comprise luminescent compounds such as dyes or whiteners. This section compares the results of analysis performed with standard (white-light) and spectrally filtered illumination to extract the fractional contribution of luminescence to loss of transparency.

As practically relevant examples of luminescent specimens, we select two series of plaques of LLDPE and PP containing varying fractions of NX8000. This commercial clarifying agent is found to additionally contain a whitener that exhibits pronounced photoluminescence (PL), as shown in **Figure 9**a. The equivalent absorption spectrum of the whitener was measured via PL excitation (PLE) spectroscopy and features a maximum at 375 nm and absorption edge at 410 nm. The corresponding PL spectrum spans 390–550 nm with a maximum at 431 nm. Thus, considering the spectral output of the respective light sources, photoexcitation of luminescence is possible for both ID- and haze-meter-based analysis, as well as under most types of ambient lighting. A 25-µm-thick Kapton film is employed as a long-pass filter due to its high transparency ($H_{ID}(0) = 1.8\%$, $S_{ID}(0) = 98.4\%$) and high absorbance for wavelengths shorter than 450 nm (Figure 9a), which eliminates the photoexcitation of luminescence for the particular whitener employed. Silica-filled PS plaques are selected as a reference, non-luminescent sample set.

$H_{ID}(8)$ and $S_{ID}(8)$ values were first recorded with unfiltered white-light illumination, obtaining the values shown previously in Figures 3 and 4b respectively. The Kapton film was then placed in contact with the graticule and the instrument was tared to baseline the readings in the absence of any sample: $H_{ID} = 0.0\%$ and $S_{ID} = 99.8\%$. Following this simple procedure, the samples were re-measured with the filtered illumination. Subtracting the respective values recorded with white-light and filtered illumination thus extracts the contribution of luminescence to ID-haze and ID-sharpness. For completeness, exemplary pre-subtraction data is given in Figure S4, Supporting Information.

The contribution of luminescence to $H_{ID}(8)$ is shown in Figure 9b plotted as a function of "total" $H_{ID}(8)$ measured with white-light illumination. Reassuringly, for non-luminescent silica-filled PS samples $H_{ID}(8)$ remains constant within experimental error. On the contrary, the contribution of luminescence can be clearly resolved for LLDPE/NX8000 and PP/NX800, increasing with $H_{ID}(8)$ and reaching 3% at $H_{ID}(8) \approx 30\%$. Interestingly, the trend is less clear when the same data is plotted as a function of the concentration of NX8000 (and, therewith, the whitener) in the samples, as shown in Figure S5. The loss of sharpness due to luminescence (Figure S6a) is highest for PP/NX8000 samples exhibiting a relatively low total haze ($H_{ID}(8) =$ 5–8%), reaching a maximum value of 2%.

The proposed interpretation for the above is based on the variation of luminescence outcoupling efficiency with specimen haze, and is illustrated schematically in Figure 9c. In fact, similar principles underlie the emerging use of hazy light-scattering substrates to improve the efficiency of organic light-emitting devices.[48–50] While the angular distribution

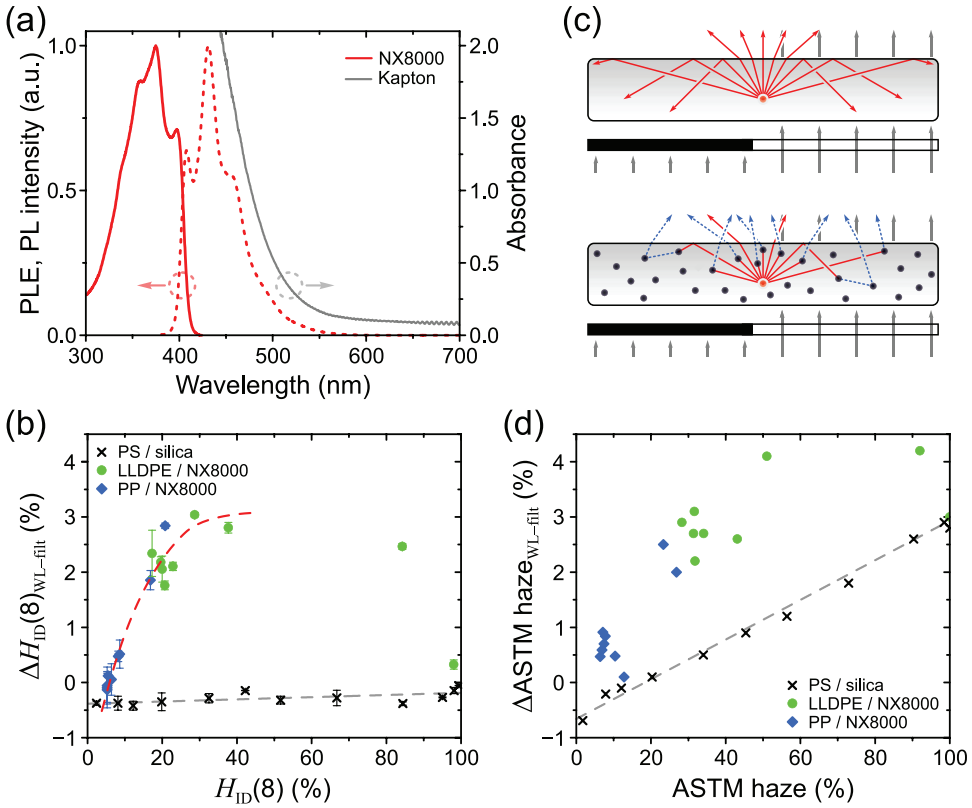

Figure 9. The effect of specimen luminescence on transparency. a) PLE and PL spectra of a commercial NX8000 additive (solid and dotted red lines respectively; left ordinate), measured for compounded blends with LLDPE. Also shown is the absorption spectrum of a Kapton polyimide film used as a long-pass filter (gray line; right ordinate). b) Contribution of luminescence to ID-haze measured at 7.9 mm airgap distance, $\Delta H_{ID}(8)$, calculated as the difference of values recorded using white-light ("WL") and filtered-light ("filt") illumination. Data is shown for plaques of LLDPE and PP containing varying fractions of NX8000, as well as non-luminescent plaques of silica-filled PS, as a function of the corresponding ID-haze recorded with WL illumination. c) Schematic of luminescence contribution to haze for maximally-transparent (top) and hazy (bottom) specimens, backlit via a graticule. Exemplary ray propagation is shown for refracted/reflected (solid red lines) and scattered (dotted blue lines) luminescence light. **d**) Contribution of luminescence to ASTM haze, calculated as in (b) for the same samples, plotted as a function of the ASTM haze recorded with WL illumination. Dashed red line in (b) is a guide to the eye; dashed gray lines in (b) and (d) are linear fits to the data for PS/silica plaques.

of luminescence is typically isotropic, light impinging the polymer-air interface at angles greater than the critical angle (e.g., 42° for LLDPE-air) will undergo total internal reflection due to the refractive index difference for the two layers. Hence, for low-haze samples most of the luminescence would not be outcoupled, resulting in only a minor contribution to loss of transparency – for example, a small loss of ID-sharpness observed for maximally clarified PP/NX8000 samples. With increasing haze, however, the probability of luminescence outcoupling increases due to multiple scattering events that can re-direct light to the interface at sub-critical angles. As illustrated in Figure 9c, the latter would indeed increase the apparent brightness of the masked regions, leading to reduced contrast for the backlit and masked regions, quantified as ID-haze.

Performing the same analysis with a conventional haze-meter similarly reveals a luminescence contribution for samples containing NX8000 (Figure 9d). However, in this case, the analysis is less reliable given that data for non-luminescent PS/silica samples also features an unexpected haze-dependent offset across the entire range of haze values. The corresponding clarity data (Figure S6b, Supporting Information) similarly yields a constant 3% offset for both luminescent and reference samples. An additional practical inconvenience of employing the conventional haze-meter was found to be the need for the instrument to be re-calibrated when optical filters are used (Figure S7, Supporting Information).

Hence, ID-based analysis is shown to provide a straightforward means of quantifying the contribution of specimen luminescence to loss of transparency, requiring only a simple tare procedure. Such analysis is particularly relevant for optimizing formulation of additive blends containing whiteners, as well as various other products, such as cosmetic substances.

4. Conclusion

While transparency represents one of the principal material characteristics, to-date it has been predominantly quantified in the field using the simplistic ASTM D1003 standard. However, its adequacy for visual-perception-correlated analysis has been questioned—particularly given that it fails to capture such

commonplace phenomena as the variation of transparency with increasing airgap distance between a turbid material and the viewed object. This study presented an alternative imaging-based method in which the ID arising due to light interacting with a turbid specimen is evaluated by comparing images of a backlit graticule recorded with and without said specimen. More specifically, ID-haze is quantified as the reduction of contrast via analysis of the corresponding ESFs, while ID-sharpness is derived from analysis of the corresponding MTFs to express the loss of detail resolution.

ID-haze and ID-sharpness are found to exhibit the expected variation with airgap distance, with a one-to-one correlation observed between ASTM haze and ID-haze measured at an 8 mm airgap for the majority of tested samples. While "clarity" measured using a standard ASTM haze-meter features a comparatively narrow dynamic range and is rarely reported in the field, simultaneous analysis of ID-sharpness and ID-haze was found to provide a more complete evaluation of transparency—describing, for instance, the tendency of ID-haze to reach plateau values with increasing airgap for high-sharpness samples. Furthermore, the use of a graticule was demonstrated to enable sensitive detection of local transparency defects and their differentiation from large-area characteristics. Finally, the use of spectrally-filtered illumination for the imaging-based method revealed an appreciable, up to 3%, contribution of luminescence to haze for polyolefin plaques clarified with a commercial additive containing a whitener.

In summary, the presented method offers numerous advantages and opens avenues for application in research and development of (semi-)transparent materials, in particular polymers and additives, therefore, targeting specific applications in terms of, for instance, the airgap intended for the observer and the relative importance of reproducing contrast or object detail. Furthermore, the method is particularly suited for on-line process and quality control, enabling rapid acquisition of optical data to maintain product quality and homogeneity. Finally, the method offers the potential for further extension to enable yet more sophisticated analysis such as, for instance, polarization-dependent transparency measurements for anisotropic specimens.

Supporting Information

Supporting Information is available from the Wiley Online Library or from the author.

Acknowledgements

The authors express their deepest gratitude to Rhopoint Instruments Ltd. for their generous loan of the Rhopoint ID-TX imaging transmission appearance meter, and Mr. Samuel Whitham (Rhopoint Instruments Ltd.) for contributing invaluable insights into ID-based analysis of haze. The authors also thank Prof. Paul Smith (ETH Zürich) for supporting this work through many fruitful discussions and critically reviewing the manuscript. Prof. Hans-Werner Schmidt (Universität Bayreuth) is acknowledged for providing access to the injection-molding facilities used for fabricating the samples studied in this work. Ms. J. Braun (ETH Zürich) and Mr. A. R. P. Lane-Mann (Boston College) are thanked for invaluable experimental input. AP acknowledges the financial support by the Federal Ministry of Education and Research (BMBF) and the Baden-Württemberg Ministry of Science as part of the Excellence Strategy of the German Federal and State Governments.

Open access funding enabled and organized by Projekt DEAL.

Conflict of Interest

The authors declare no conflict of interest.

Data Availability Statement

The data that support the findings of this study are available from the corresponding author upon reasonable request.

Keywords

clarifying agents, clarity, haze, light scattering, optical properties, roughness, transparency

Received: January 21, 2021
Revised: February 28, 2021
Published online: March 24, 2021

[1] Y. Lin, E. Bilotti, C. W. M. Bastiaansen, T. Peijs, *Polym. Eng. Sci.* **2020**, *60*, 2351.
[2] B. A. Morris, *The Science and Technology of Flexible Packaging: Multilayer Films from Resin and Process to End Use*, Elsevier, Amsterdam **2016**.
[3] G. H. Meeten, *Optical Properties of Polymers*, Elsevier Applied Science Publishers, Amsterdam **1986**.
[4] ASTM D1003-13, *Standard Test Method for Haze and Luminous Transmittance of Transparent Plastics*, **2013**.
[5] F. C. Stehling, C. S. Speed, L. Westerman, *Macromolecules* **1981**, *14*, 698.
[6] E. Andreassen, A. Larsen, K. Nord-Varhaug, M. Skar, H. Øysæd, *Polym. Eng. Sci.* **2002**, *42*, 1082.
[7] X. Liu, X. Dong, Y. Xiong, P. Yi, Y. Ren, S. Guo, *J. Appl. Polym. Sci.* **2016**, *133*, 44156.
[8] Y. Zhang, F. Li, Q. Yu, C. Ni, X. Gu, Y. Li, J. You, *Macromol. Mater. Eng.* **2019**, *304*, 1900316.
[9] J. Molnár, Ö. Sepsi, G. Erdei, S. Lenk, F. Ujhelyi, A. Menyhárd, *J. Polym. Sci.* **2020**, *58*, 1787.
[10] D. V. Rosato, *Extruding Plastics: A Practical Processing Handbook*, Springer-Science, Berlin, Germany **1998**.
[11] C. Habel, M. Schöttle, M. Daab, N. J. Eichstaedt, D. Wagner, H. Bakhshi, S. Agarwal, M. A. Horn, J. Breu, *Macromol. Mater. Eng.* **2018**, *303*, 1800333.
[12] R. H. French, J. M. Rodríguez-Parada, M. K.Yang, R. A. Derryberry, N. T. Pfeiffenberger, *Sol. Energy Mater. Sol. Cells* **2011**, *95*, 2077.
[13] G. Wu, W. Li, W. Ni, L. Chen, G. Sun, B. You, *Macromol. Mater. Eng.* **2019**, *304*, 1900174.
[14] Y.-W. Lim, J. Jin, B.-S. Bae, *Adv. Mater.* **2020**, *32*, 1907143.
[15] P. L. Marasco, H. L. Task, *Proc. SPIE* **1999**, *3689*, 2.
[16] P. L. Marasco, H. L. Task, *Proc. SPIE* **2001**, *4361*, 188.
[17] M. A. Guevara, W. R. Brockmeier, T. K. Kuyk, P. A. Smith, B. P. Goettl, B. J. Novar, Technical report No. AFRL-RH-FSTR-2017-0022, https://apps.dtic.mil/docs/citations/AD1040196, (accessed: January, 2021).
[18] C. A. Williamson, L. N. McLin, M. A. Manka, J. M. Rickman, P. V. Garcia, P. A. Smith, *Opt. Express* **2018**, *26*, 27033.

[19] R. J. Tabar, C. T. Murray, R. S. Stein, *J. Polym. Sci., Polym. Phys. Ed.* **1983**, *21*, 831.
[20] ASTM D1746–15, *Standard Test Method for Transparency of Plastic Sheeting*, **2015**.
[21] S. Wimmer, P. Schwarz, BYK-Gardner GmbH, *US8749791*, **2014**.
[22] Z. Yu, Y. Xu, K. Qiao, L. Zhang, Z. Chen, X. Yang, A. Ji, M. Wu, Y. Gao, *Macromol. Mater. Eng.* **2018**, *303*, 1800142.
[23] A. Perevedentsev, M. Campoy-Quiles, *Nat. Commun.* **2020**, *11*, 3610.
[24] Z. Fang, H. Zhu, Y. Yuan, D. Ha, S. Zhu, C. Preston, Q. Chen, Y. Li, X. Han, S. Lee, G. Chen, T. Li, J. Munday, J. Huang, L. Hu, *Nano Lett.* **2014**, *14*, 765.
[25] J. Ham, W. J. Dong, G. Ho, J.-L. Jung, *ACS Appl. Mater. Interfaces* **2016**, *8*, 5990.
[26] Y. Yao, J. Tao, J. Zou, B. Zhang, T. Li, J. Dai, M. Zhu, S. Wang, K. K. Fu, D. Henderson, E. Hitz, J. Peng, L. Hu, *Energy Environ. Sci.* **2016**, *9*, 2278.
[27] J. Shen, F. Li, Z. Cao, D. Barat, G. Tu, *ACS Appl. Mater. Interfaces* **2017**, *9*, 14990.
[28] T. Magrini, F. Bouville, A. Lauria, H. L.e Ferrand, T. P. Niebel, A. R. Studart, *Nat. Commun.* **2019**, *10*, 2794.
[29] A. Perevedentsev, F. L. Bargardi, A. Sánchez-Ferrer, N. J. Cheetham, A. Sousaraei, S. Busato, J. Gierschner, B. Milián-Medina, R. Mezzenga, R. Wannemacher, J. Cabanillas-Gonzalez, M. Campoy-Quiles, W. R. Caseri, *ACS Omega* **2019**, *4*, 10192.
[30] J. Y. Park, W. S. Cho, C. S. Choi, S.-H. Cho, J.-L. Lee, *Adv. Opt. Mater.* **2020**, *8*, 1901866.
[31] S. Busato, A. Perevedentsev, *Polym. Eng. Sci.* **2017**, *58*, 345.
[32] M. Kristiansen, M. Werner, T. Tervoort, P. Smith, M. Blomenhofer, H.-W. Schmidt, *Macromolecules* **2003**, *36*, 5150.
[33] F. Abraham, S. Ganzleben, D. Hanft, P. Smith, H.-W. Schmidt, *Macromol. Chem. Phys.* **2010**, *211*, 171.
[34] Rhopoint ID Imaging Transmission Meter, https://www.rhopointinstruments.com/product/rhopoint_id_imaging_transmission_meter, (accessed: January, 2021).
[35] Public-domain software, ImageJ: Image Processing and Analysis in Java, http://imagej.nih.gov/ij/, (accessed: January, 2021).
[36] ImageJ plugin, Slanted Edge MTF, https://imagej.nih.gov/ij/plugins/se-mtf/index.html, (accessed: January, 2021).
[37] C. M. Fratini, *Doctoral Thesis*, Virginia Polytechnic Institute and State University, Blacksburg, VA **2006**.
[38] A. Perevedentsev, S. Aksel, K. Feldman, P. Smith, P. N. Stavrinou, D. D. C. Bradley, *J. Polym. Sci., Part B: Polym. Phys.* **2015**, *53*, 22.
[39] ISO 12233, (Third edition), *Photography – Electronic Still Picture Imaging – Resolution and Spatial Frequency Responses*, **2017**.
[40] A. K. R. Choudhury, *Principle of Colour Appearance and Measurement*, Woodhead Publishing, Cambridge **2014**.
[41] H. Kukkonen, J. Rovamo, K. Tiippana, R. Näsänen, *Vision Res.* **1993**, *33*, 1431.
[42] X.-J. Gu, M. Hu, B. Li, X.-T. Hu, *PLoS One* **2014**, *9*, e86542.
[43] S. Idrees, M. P. Baumann, F. Franke, T. A. Münch, Z. M. Hafed, *Nat. Commun.* **2020**, *11*, 1977.
[44] Z. W. Wilchinsky, *J. Appl. Polym. Sci.* **1961**, *5*, 48.
[45] G. D. Boreman, *Modulation Transfer Function in Optical and Electro-Optical Systems*, SPIE Press, Bellingham **2001**.
[46] H. Weber, *Digitale Farben in der Medienproduktion und Druckvorstufe*, MITP Verlag, Heidelberg **2006**.
[47] W.-C. Liu, J. Hwang, A. Koo, H. Wu, R. Leecharoen, H.-L. Yu, *J. Phys.: Conf. Ser.* **2018**, *972*, 012023.
[48] E. Kim, H. Cho, K. Kim, T.-W. Koh, J. Chung, J. Lee, Y. Park, S. Yoo, *Adv. Mater.* **2015**, *27*, 1624.
[49] T.-W. Koh, J. A. Spechler, K. M. Lee, C. B. Arnold, B. P. Rand, *ACS Photonics* **2015**, *2*, 1366.
[50] K. Tong, X. Liu, F. Zhao, D. Chen, Q. Pei, *Adv. Opt. Mater.* **2017**, *5*, 1700307.